Heliyon

Received:
10 December 2018
Revised:
25 March 2019
Accepted:
27 March 2019

Cite as:
Carlos Zambra. Simulation of mass transfer in hollow fiber used for concentration of juices by osmotic distillation. Heliyon 5 (2019) e01458.
doi: 10.1016/j.heliyon.2019.e01458

Simulation of mass transfer in hollow fiber used for concentration of juices by osmotic distillation

Carlos Zambra*

Department of Mechanical Engineering, Universidad de Talca, Curicó, Chile

* Corresponding author.
E-mail address: czambra@utalca.cl (C. Zambra).

Abstract

A bi-dimensional diffusion mathematical model is proposed to study mass transfer in hollow fiber used for the concentration of juices by osmotic distillation (OD). The mathematical model was solved using the Finite Volume Method (FVM). The mass fraction at the boundaries was calculated by using the Functional-group Activity Coefficients (UNIFAC) method for the juice and by the Analytical Solutions Of Groups (ASOG) method for the brine. Calculated results were compared to an analytical solution for a case of mass diffusion in a cylinder with mass flow boundary condition. An algorithm to find the effective diffusion coefficient of gas through the membrane is proposed. To show its usefulness, different velocities were applied over the fiber surface to study the bi-dimensional effects that this velocity field has on the mass transfer inside the fiber. The results showed a maximum error of 5.6% when compared to experimental results.

Keywords: Theoretical chemistry, Food science, Chemical engineering

https://doi.org/10.1016/j.heliyon.2019.e01458

1. Introduction

Osmotic distillation (OD) is a process that uses hydrophobic membranes to isolate feed liquid from a concentrated brine. Hollow fibers of cylindrical form are the most commonly-used membranes in OD. Commercial modules that group these fibers have been used in several experimental studies of juice concentration (Cassano and Drioli, 2007; Dincer et al., 2016; Hasanoğlu et al., 2012; Valdés et al., 2009). The importance of the OD as process lies on the fact that it enables to preserve and concentrate the nutritional properties of foods, and it decreases aromatic compound losses (Cisse et al., 2005; Vaillant et al., 2001). OD is essentially a gas transport process through a membrane. This gas is composed by water vapor and other volatile compounds contained in the feed liquid (Dincer et al., 2016; Liguori et al., 2013). An osmotic agent with low water activity, also called extractant solution or brine, is used to generate a concentration gradient that causes gaseous-state mass transfer from the feed liquid. Several extractant have been studied; however, calcium chloride is the most used due to its low cost (Celere and Gostoli, 2005; Savaş Bahçeci et al., 2015).

Mathematical models have been proposed to calculate transmembrane fluxes and concentrations in membrane separation processes (Rana et al., 2015, 2014). The existing to describe and improve the OD process go from empirical correlations (Woods and Pellegrino, 2013), simple mathematical models (e.g: resistance in series) (Ruiz Salmón et al., 2017) up to complex turbulent three dimensional models (Computational Fluid Dynamics, CFD). The model of resistance in series of heat and mass transfer is one of the most used as was noticed by Rana and Matsuura (2010). Its application has previously been reported in the literature in simulations of heat and mass transfer for OD in noni juice (Valdés et al., 2009). In this work was considered the thermodynamic phenomena of phase change and both heat and mass transfer to calculate the flow rates going through the membrane. The resistance in series model only utilizes the total transfer surface area, therefore does not consider membrane geometry or local velocity field. CFD tackles these two existing issues in the resistance in series model. CFD allows the study of *local* variations of velocity and temperature considering bi-dimensional and tri-dimensional membrane geometry. CFD studies of the fluid dynamics on hollow fibers inside a commercial membrane module have demonstrated that the configuration of these modules does not yield homogeneous distributions of velocity along the surface of fibers (Kaya et al., 2014). Therefore, it can be inferred that mass transfer has a different behavior in each fiber depending on the spatial location inside the module. Recent studies have modified the geometry of hollow fiber in order to increase the advection, and in this way, also improve mass transfer (Luelf et al., 2017; Motevalian et al., 2016). These studies have shown the need to consider the local velocity field on the fiber to improve mass transfer calculation. The above-mentioned studies consider the vapor

https://doi.org/10.1016/j.heliyon.2019.e01458

water diffusion coefficient in the air to calculate the mass flow through the fiber. This is common practice, but it constitutes a source of error, because the evaporating gas does not only contain water, but also other volatiles compounds, such as polyphenols. Additionally, the diffusion coefficient may vary during the OD process because of concentration changes in both the feed liquid and the brine. In order to improve the accuracy of the currently existing models, we proposes to incorporate an effective gas diffusion coefficient flowing through the membrane that varies along with the mass fraction of the liquid being fed. This effective diffusion coefficient can be calculated using an inverse problem, provided that the mass flow rates, which depend on the concentration in equilibrium in the membrane edges, are known. The calculation of phase equilibrium at the boundaries liquid-gas (feed-membrane) and gas-liquid (membrane-extractant) is rather complex. Models such as the Analytical Solutions of Groups (ASOG) (Correa et al., 1997) and UNIFAC (Peres and Macedo, 1999) have been proposed to predict the phase equilibrium by water activity calculation for brine solution and for aqueous sugar solutions, respectively. To improve the calculation and analysis of the OD process, this article proposes a new algorithm that groups three calculation methods. The methods used are presented in what follows.

i. In order to obtain the membrane boundary conditions, the UNIFAC and ASOG methods were used. These methods make it possible to find at each control volume the concentration of gas and liquid in the equilibrium on both sides of the membrane at each time step.
ii. In order to calculate the diffusion of the mixture of gases through the membrane, an iterative algorithm to find the effective diffusion coefficient at each time step was developed. The algorithm is supplied by the mass flow rates calculated with the water mass convection equation from the inside of the fluid to the edge of the membrane. The liquid mass fraction that evaporates on this edge is calculated considering the liquid-gas phase equilibrium (ASOG and UNIFAC) in the edges of the membrane.
iii. In order to consider the local effect that different velocity fields have over the surfaces of the hollow fiber in the mass distribution inside of the membrane, a diffusion bi-dimensional mathematical model was solved by using FVM (Patankar, 1991).

A test case of concentration of cranberry juice by OD was performed. The calculated numerical results were then compared to the resistance in series model obtained from previous studies. To demonstrate the applicability and precision of the algorithm developed, three non-uniform velocity fields were applied on the surface of the membrane. These results allowed us to study the distribution of the concentrations inside the membrane produced by non-uniform velocities at the edges.

https://doi.org/10.1016/j.heliyon.2019.e01458

2. Model

Fig. 1 shows the physical geometry used in this study, which corresponds to a hollow fiber of cylindrical shape located inside of a membrane module. The brine flows through the inner side of the fiber (zone 3 in Fig. 1c) while the feed (juice) flows outside of it (zone 1 in Fig. 1c). The mass transfer through the hydrophobic membrane occurs due to a phase change liquid-gas (zone 2 in Fig. 1c). The simulation in the current study was conducted on a single hollow fiber. The dimensions of the hollow fiber used in this study can be found in Table 1.

3. Theory/calculation

The physical layout presented in Fig. 1c can be modelled by an unsteady bi-dimensional mathematical model in polar coordinates. The corresponding equation can be expressed as:

$$\frac{\partial X_s}{\partial t} = \frac{1}{r}\frac{\partial}{\partial r}\left(\frac{\varepsilon}{\tau} Dwa(X_s,p) r \frac{\partial X_s}{\partial r}\right) + \frac{1}{r^2}\frac{\partial}{\partial \theta}\left(\frac{\varepsilon}{\tau} Dwa(X_s,p)\frac{\partial X_s}{\partial \theta}\right). \quad (1)$$

where the diffusion coefficient $Dwa(X_s,p)$ corresponds to the capacity of the water vapor and volatile compounds (gas) to spread through the membrane as function of the mass fraction of gas inside the membrane (X_s) and the osmotic pressure (p), and where r is the hollow fiber radius, and θ is the angular coordinate. In order to calculate an effective diffusion coefficient that includes porosity (ε) and tortuosity (τ), the following equation is proposed:

$$\frac{\partial X_s}{\partial t} = Dwa\left(X_b^1\right)\left(\frac{\partial^2 X_s}{\partial r^2} + \frac{1}{r^2}\frac{\partial^2 X_s}{\partial \theta^2}\right). \quad (2)$$

where $Dwa(X_b^1)$ is the effective diffusion coefficient and X_b^1 is the total suspended solid or brix degree in the feed.

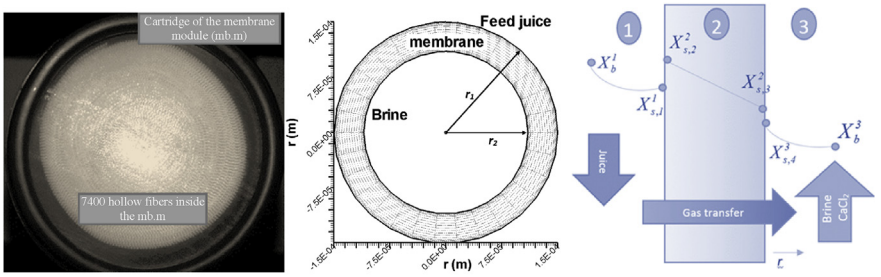

(a) (b) (c)

Fig. 1. Physical layout used for the numerical study: (a) Top view of a commercial fiber module (7400 fibers); (b) physical layout considered in this study (one fiber); (c) a scheme of the membrane that includes the used nomenclature in the mathematical model for the mass transfer.

https://doi.org/10.1016/j.heliyon.2019.e01458

Table 1. Data sheet of the commercial membrane contactor used for OD.

Fiber type	**Celgard® microporous, polypropylene 1.7 × 5.5 membrane contactor**
External diameter (m)	3.0E-4
Internal diameter (m)	2.2E-4
Length (m)	0.12
Estimated number of fiber	7400
Porosity (ε)	0.4
Tortuosity (τ)	3.92
Catridge characteristics	
Cartridge dimensions (D x L) (m × m)	0.043 × 0.114
Effective external surface area (m^2)	0.58

Initially, a constant concentration of gas $X_s(x,\theta,0) = X_{in}^2 = 0$ was considered inside the membrane. Water convective flux from the juice to the interphase with the membrane (Jw^1) and from the membrane interphase to the brine (Jw^3) are calculated with the following equations:

$$Jw^1 = h_m^{(1)} \cdot \rho_{v,w} \cdot \left(X_b^{(1)} - X_{s,1}^{(1)}\right) \quad \text{at } r = r_1, \tag{3}$$

$$Jw^3 = h_m^{(3)} \cdot \rho_{v,w} \cdot \left(X_{s,4}^{(3)} - X_b^{(3)}\right) \quad \text{at } r = r_2. \tag{4}$$

where $\rho_{v,w}$ is water vapor density at the corresponding temperature and the superscript (1) and (3) are the mass convection coefficient and the concentration in the feed and brine respectively. The mass fraction values $X_{s,4}^{(3)}$ and $X_{s,1}^{(1)}$ for brine and juice were obtained from ASOG and UNIFAC methods, respectively. In these methods, the properties are obtained considering a solution of saccharose for the juice, and a solution of $CaCl_2$ for the brine. In Eqs. (3) and (4), the values of the convection mass coefficient (h_m) were obtained from the Sherwood number (Sh). The correlation suggested by Gabelman and Hwang (1999) was used for the juice flowing by the shellside of the membrane contactor:

$$Sh^{(1)} = 0.019Gz. \tag{5}$$

The Eq. (5) was developed for a flow parallel to the fibers in close-packed fibers and when the Graetz number (Gz) is less than 60. The Sherwood number for the brine was estimated by Eq. (6).

$$Sh^{(3)} = 0.0149\left(\mathrm{Re}^{(3)}\right)^{0.88}\left(Sc^{(3)}\right)^{1/3}. \tag{6}$$

This equation considers laminar flow conditions and it is applicable if the Schmidt number (Sc) $\geq$ 100 (Zambra et al., 2014).

https://doi.org/10.1016/j.heliyon.2019.e01458

4. Methodology

The mathematical model is solved by the finite volume method (FVM) (Patankar, 1991), which discretizes the general transport equation for a bi-dimensional diffusion transient model (for further details, see (Zambra and Moraga, 2013)). The calculations were carried out with our own code written in Fortran. Tests were conducted by using meshes of *64 x 64* and *32 x 32* nodes, and at $\Delta t = 1\ s$ and $\Delta t = 10\ s$ time steps. Results showed that the relative errors were smaller than 1E-4 for the tested case (see section 5). Therefore, in all cases the used time step was 10 s and the mesh *32 x 32* nodes in $r \times \theta$ direction. The local flow rate at the membrane interface (Jw_{t,FVM,r_1}) was calculated directly from the code using the discretized equation:

$$Jw_{t,FVM,r_1} = -\frac{\varepsilon}{\tau} Dwa(X_s,p)\frac{\Delta X_s}{\Delta r}\bigg|_{r=r_1,\theta} \tag{8}$$

It should be remembered that in accordance with the mass balance, the gas flux going into the membrane from the juice-membrane interphase has to be the same as the one coming out of the interphase membrane-brine. The numerical value of Jw_{t,FVM,r_1}, calculated by Eq. (8), has units of m s^{-1}, and therefore, it must be multiplied by the density of the gas ($\rho_{v,w}$) and divided by the flow area (A_{ext}) in order to calculate the global transmembrane flow in consistent units. In this study, the external area (A_{ext}) of the membrane is chosen arbitrarily to calculate the flow. Density is assigned the value of water vapor. Under these considerations, the global numerical transmembrane flow can be calculated with the following formula:

$$Jw^2 = \frac{Jw_{t,FVM,r_1} \cdot \rho_{v,w}}{A_{ext}} \left(\mathrm{kg\ m^{-2}\ s^{-1}}\right). \tag{9}$$

4.1. Analysis

In order to find errors between experimental or exact solutions and the obtained numerical results, the integral of each obtained curve was calculated by using the least square method. The integrals were calculated using the trapezoidal method of second-order accuracy. Thus, the relative error (RE) at time t is defined by the following equation (Zambra et al., 2015):

$$RE = \frac{\left| \int_{y=0}^{y=\max} f(x,y)_{t,FVM}\mathrm{d}y - \int_{y=0}^{y=\max} f(x,y)_{t,ex}\mathrm{d}y \right|}{\left| \int_{y=0}^{y=\max} f(x,y)_{t,ex}\mathrm{d}y \right|}. \tag{10}$$

https://doi.org/10.1016/j.heliyon.2019.e01458

4.2. Calculation

An inverse method was used to obtain the diffusion coefficient. The calculation algorithms is summarized in Fig. 2. These algorithms were supplied by the data of the water convective flux at the boundary ($Jw^{(1)}$) obtained from Eq. (3). This flux was compared to the calculated value from the FVM ($Jw^{(2)}$), Eq. (9). The algorithm takes a maximum error (Δerr), between $Jw^{(1)}$ and $Jw^{(2)}$ of 1E-4. As a result of the algorithm developed, the gas diffusion coefficient inside of the membrane $\frac{\varepsilon}{\tau}Dwa(X_s,p)$ is obtained for each time step Δt. The resulting values are used to obtain the effective diffusion coefficient $Dwa(X_b^{(1)})$. This effective variable coefficient was adjusted with the following exponential function (Serrano, 2004):

$$\frac{\varepsilon}{\tau}Dwa(X_s,p)\approx Dwa\left(X_b^{(1)}\right)=\vartheta_1 e^{\lambda\left(X_b^{(1)}\right)^{\alpha}}-\vartheta_2. \tag{11}$$

where symbols $\vartheta 1$, $\vartheta 2$, λ and α are adjustment coefficients.

The accuracy of the algorithm developed to calculate the values of the effective diffusion coefficient $Dwa(X_b^{(1)})$ depends on the precision of the numerical method.

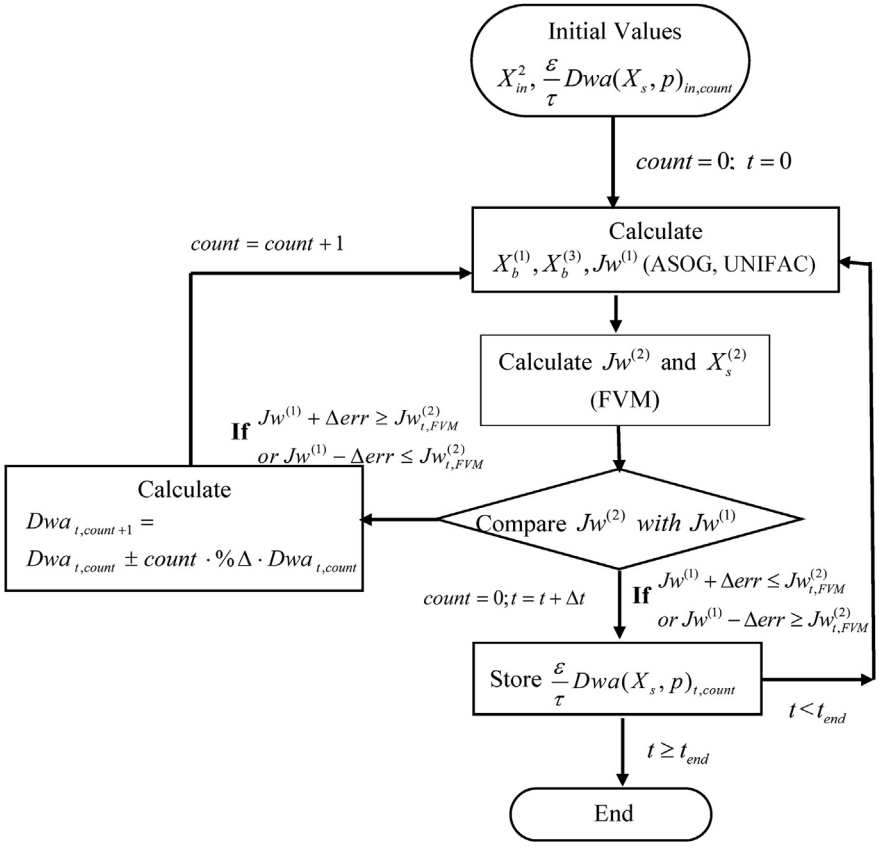

Fig. 2. Scheme of the algorithms used to obtain the effective diffusion coefficient inside the membrane.

https://doi.org/10.1016/j.heliyon.2019.e01458

In the next section, we study the accuracy of FVM to solve an approximate problem of diffusion in a cylinder.

5. Example

It is well-known that the classical finite volume developed by Patankar (1991) is highly accurate to solve problems when the pressure field is known or the main transport mechanism is diffusion. Given that one of the aims of this study is to find the effective diffusion coefficient with the best possible accuracy, results of a sensitivity test for a non-stationary, bi-dimensional mass diffusion in a cylinder are presented. This case was chosen, because the simulation results can be compared to 1D exact solutions, and both geometrical and boundary conditions are similar to those used to solve the mass flux in hollow fiber membranes. A long cylinder with mass flux boundary conditions is considered. If initially the surface has a uniform concentration of $X_{s,1}^{(1)}(r_1,\theta,0) = X_{in}$, and it is suddenly immersed in a fluid which is under convection conditions, then the boundary condition at each time step may be expressed as:

$$Dwa\left.\frac{dX}{dr}\right|_{r=r_1} = h_m\left(X_{s,1}^{(1)} - X_b\right), \tag{12}$$

where X_b is the concentration of the fluid over cylinder, $X_{s,1}^{(1)}$ is the concentration at the surface of cylinder at time t, h_m is the convection mass coefficient and Dwa is the diffusion mass coefficient. The equation to solve this problem in two dimensions is:

$$\frac{\partial X}{\partial t} = Dwa\left(\frac{\partial^2 X}{\partial r^2} + \frac{1}{r^2}\frac{\partial^2 X}{\partial \theta^2}\right). \tag{13}$$

It is reasonable to assume one-dimensional diffusion in r-direction (infinite cylinder case $L/r_1 \geq 10$) and an analytical solution may be found for the concentration profile in r-direction. For this unsteady diffusion problem the solution for the concentration profile is (Bergman et al., 2011):

$$X^* = \sum_{n=1}^{\infty} C_n \exp\left(-\zeta_n^2 Fo_m\right) J_0\left(\zeta_n r^*\right);\ C_n = \frac{2}{\zeta_n}\frac{J_1(\zeta_n)}{J_0^2(\zeta_n) + J_1^2(\zeta_n)};\ Fo_m = \frac{Dwa \cdot t}{r_1^2}. \tag{14}$$

where Fo_m is the mass Fourier number, J_1 and J_0 are the Bessel functions of first kind and their values may be obtained from tables. The discrete values of ζ_n are positive roots of the transcendental equation $\zeta_n \frac{J_1(\zeta_n)}{J_0(\zeta_n)} = Bi_m$, where the mass Biot number (Bi_m) is used. For this case $Dwa = 5\text{E-}10\ \text{m}^2\ \text{s}^{-1}$, $h_m = 1.3\text{E-}6\ \text{m s}^{-1}$, $X_{w,i} = 0$ and $X_b = 0.7$. Fig. 3 shows a comparison between analytical and simulated results with a mesh of 32 × 32 nodes in $r \times \theta$ direction and time step of 10 s.

https://doi.org/10.1016/j.heliyon.2019.e01458

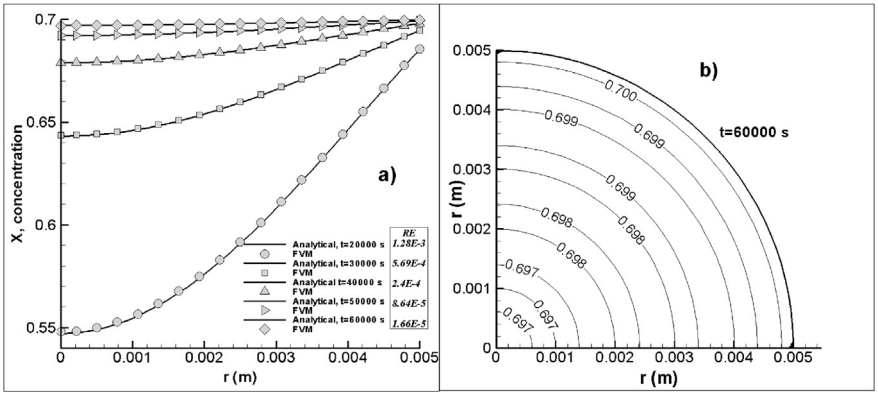

Fig. 3. (a) Comparison between analytic and numerical solutions with the FVM for unsteady mass transfer; (b) bi-dimensional concentration distribution inside the cylinder calculated with the FVM (1/4 of the calculate domain).

The radius of the cylinder is 0.005 m. The results presented in Fig. 3a show small relative errors for all times. The maximum was found at 20000 s and RE = 1.28E-3 (less than 0.13%). Fig. 3b shows that, for this case, the mass diffusion occurs in a radial direction and does not vary angularly, as expected.

The results shown in the previous case confirm that it is possible to obtain accurate results for unsteady diffusion problems in a cylinder with advection boundary conditions.

6. Results & discussion

The concentration of cranberry juice by OD was simulated and compared to experimental results obtained from previous work (Zambra et al., 2014). A commercial membrane module of polypropylene was used for the experimental studies. Relevant characteristics for the simulations are listed in Table 1. The values on this table were used to obtain the global values of volume decrease and the variation of mass fraction in the juice and in the brine. These obtained values were used to compare the calculated results of this study with experimental results. The process variables were flow velocity (0.5 l min^{-1}, 1 l min^{-1} and 1.5 l min^{-1}), initial brine concentration (33.13 %w/w and 39.6 %w/w) and temperature (30 °C and 40 °C). The viscosity values of the brine vary from 1.45E-3 Pa s to 6.55E-3 Pa s for a concentration range between 33.13 %w/w and 39.6 %w/w. For the cranberry juice a constant value of 0.9895 Pa s was used. The juice flows by the shellside (Zone 1 in Fig. 1c) and the brine on the inner side (Zone 3 in Fig. 1c). Initially, 0.25 l of juice and 1 l of brine were used. At each run, the test ends when the volume of the juice reaches 0.05 l.

The first study was carried out by applying a unique velocity field as boundary condition for the interface juice-membrane. The data in Table 1 was used to calculate the velocity with which the fluid flows on the inside of the module. This data was

https://doi.org/10.1016/j.heliyon.2019.e01458

applied as homogenous boundary condition on the surface of the membrane. For example, volumetric flows of 0.5 l min^{-1} and 1.5 l min^{-1} create velocity fields of 1.13E-2 m s^{-1} and 8.89E-2 m s^{-1} on the external surface of the membrane, respectively. This velocity was used to calculate the Sherwood numbers (Eqs. (5) and (6)) and the fluxes in both sides of the membrane. Fig. 4 shows the calculated variation of the mass fraction of the juice and the brine, and it also compares the volume decrease calculated in this study for the juice to the experimental results obtained from the reference. Additionally, Fig. 4f, 4h, 4j and 4l include the numerical results that were calculated by using the classical resistance in series model (Zambra et al., 2014). The RE between experimental and calculated values of the juice volume decrease were smaller than 5.6E-2 (5.6%). This is considered an important improvement, since in previous studies, errors exceeded 25% (Zambra et al., 2014). In general, it is observed that the increase of temperature, brine concentration and flow velocity cause the volume of the juice to decrease at a faster pace. The results showed that juice concentration curve (brix degree) has an exponential shape, which is in agreement with previously experimental studies of OD of juice (Cassano and Drioli, 2007). From the observation of the concentration curves, initially no sudden change in the juice concentration are expected. These curves can be used to determine the time at which the juice reached some predetermined concentration (brix degrees). This would allow for the calculation of the amount of salt ($CaCl_2$) that should

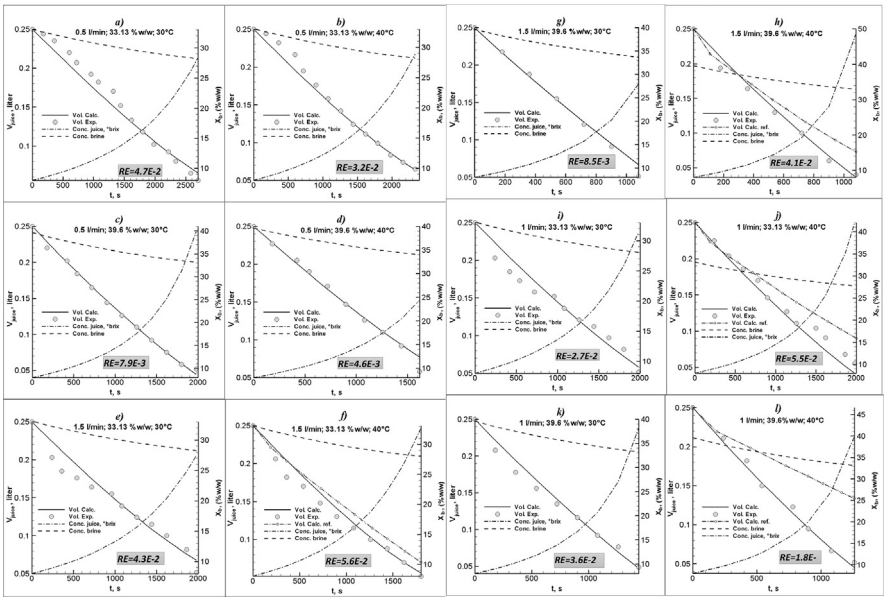

Fig. 4. Comparison of volume variation of experimental cranberry juice calculated with FVM, and time evolution of the mass fraction (%w/w) in the juice and the brine for volume fluxes of 0.5 l/min (figures a), b), c) and d)), 1 l/min (figures i), j), k) and l)), and 1.5 l/min (figures e), f), g) and h)), brine concentrations of 33.13 %w/w (figures a), b), e), f), i) and j)) and 39.6%w/w (figures c), d), g), h), k) and l)), and temperatures of 30 °C (figures a), c), e), g), i) and k)) and 40 °C (figures b), d), f), h), j) and l)). Figures f), h), j) and l), include the volume calculated with the resistance in series model (Zambra et al., 2014).

https://doi.org/10.1016/j.heliyon.2019.e01458

be added to the brine to increase its concentration up to a certain level, and consequently, continue to concentrate the juice at a determined rate.

Fig. 5 shows the calculated effective diffusion coefficient for a volumetric flow of 0.5 l/min, concentration brine of 33.13%w/w and 40 °C. The constants used in Eq. (11) are, $\vartheta_1 = 2.69E-6$, $\vartheta_2 = 0$, $\lambda = -7.8E-4$ and, $\alpha = 2$. The values vary between 2.56E-6 $m^2\ s^{-1}$ and 1.36E-6 $m^2\ s^{-1}$. The calculated values of $Dwa(X_s, p)$ are between 2.51E-5 $m^2\ s^{-1}$ and 1.33E-5 $m^2\ s^{-1}$. This indicates that there is an error when using a constant value of the air vapor diffusion coefficient.

Due to the manufacturing design of the membrane modules, areas with different velocities can be found. Non-homogeneous velocity fields are produced on the fibers' surface. The behavior of these velocity fields can be observed inside the hollow fiber modules in a study done by (Kaya et al., 2014). In this study, it was possible to observe areas of both high and low velocities on the surface of the fiber. The mass transfer (gas) through the membrane is affected by these non-homogeneous velocity fields. There is a close relation between the local mass transfer coefficient by convection and local surface velocities. A last numerical case was studied using a volumetric flow of 0.5 l min^{-1}, concentration brine of 33.13%w/w, temperature of 40 °C and two zones with different superficial velocities. The objective was to apply

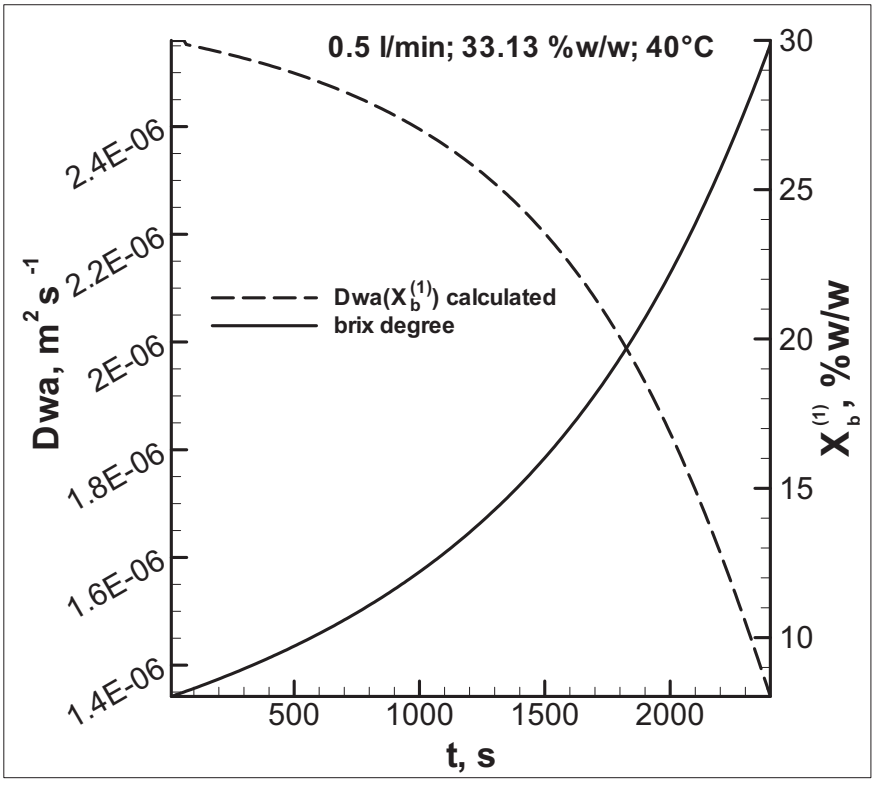

Fig. 5. Time evolution of the effective diffusion coefficient and mass fraction coefficient for concentration of cranberry juice (case b) in Fig. 4).

https://doi.org/10.1016/j.heliyon.2019.e01458

zones of high and low velocities on the external surface of hollow fibers and quantify the effects on the gas mass fraction distribution inside the membrane. Three cases of superficial velocity fields are presented. The velocities values on zone (a) were 4.32E-2 m s^{-1} (case 1), 3.18E-2 m s^{-1} (case 2) and 2.04E-2 m s^{-1} (case 3). For the three cases, the velocity value on zone (b) was 9.09E-3 m s^{-1}. The results of the gas mass fraction at different times are presented in Fig. 6. A larger mass fraction of gas is transferred into the membrane from the higher velocity zone (a). After 1 min (case 1), 1.6 min (case 2) and 2.6 min (case 3), the mass fractions on the external surface of the membrane in this zone (a) are 37.3 %w/w, 32 %w/w and 25.9 %w/w, respectively. These values in decreasing order go in line with the velocities that were imposed, also in decreasing order, which indicates coherence in the results. On this zone (a) and at the same minutes, the concentration at the internal surface of the membrane reaches maximums of 78.7 %w/w, 77.1 %w/w and 74.5 %w/w for the cases 1, 2 and 3, respectively. On the internal surface of zone (a), the gas accumulates, because the brine may not incorporate more gas in the liquid phase. At these same times, on the low velocity zones (b) a constant mass fraction of 16.5 %w/w is observed, since superficial velocity imposed in this area was the same for all cases. For cases 1, 2 and 3 in the second column of Fig. 6, the gas mass fractions inside the membrane when steady state is reached are presented. The times at which this occurs are 22.3 min, 25.5 min and 39.6 min. The steady distribution occurs, because the saccharose mass fraction in juice increases (brix degrees) and hence the fraction of water in juice decreases, while in the interior of the hollow fiber the brine is diluted and so decreases its ability (osmotic potential) to incorporate more water. The saturation pressure of both solutions tends to be equalized, so that the liquid-gas phase change rate necessary for the mass transfer through the membrane decreases. This makes the effect of the fluid velocity negligible for the mass transfer. The steady state is evident while observing the gas mass fraction values which on the external surface, in all cases, reach approximately the same value, 22.6 %w/w, but at different times while on the inner surface, these are slightly different: 73.5 %w/w, 72.1 %w/w and 71 %w/w for cases 1, 2 and 3 respectively.

From the results of the simulations, it can be confirmed that the inhomogeneous distribution of velocities on the outer surface of the hydrophobic hollow fiber membranes affects mass transfer significantly, but only at the beginning of the process when there is a high concentration of water available to be evaporated. Given that the water in the juice decreases and the brine is diluted, the vapor pressures of the juice and brine tend to balance. The distribution of the gas mass fraction inside the membrane becomes one dimensional and the velocities on the surface of the fiber becomes less relevant.

From the results of this work, it is possible to visualize the effects that different flow velocities on the surface of a hollow fiber can have on gas mass transfer inside it. From these observations, the designs to favor the maximum velocities distribution

https://doi.org/10.1016/j.heliyon.2019.e01458

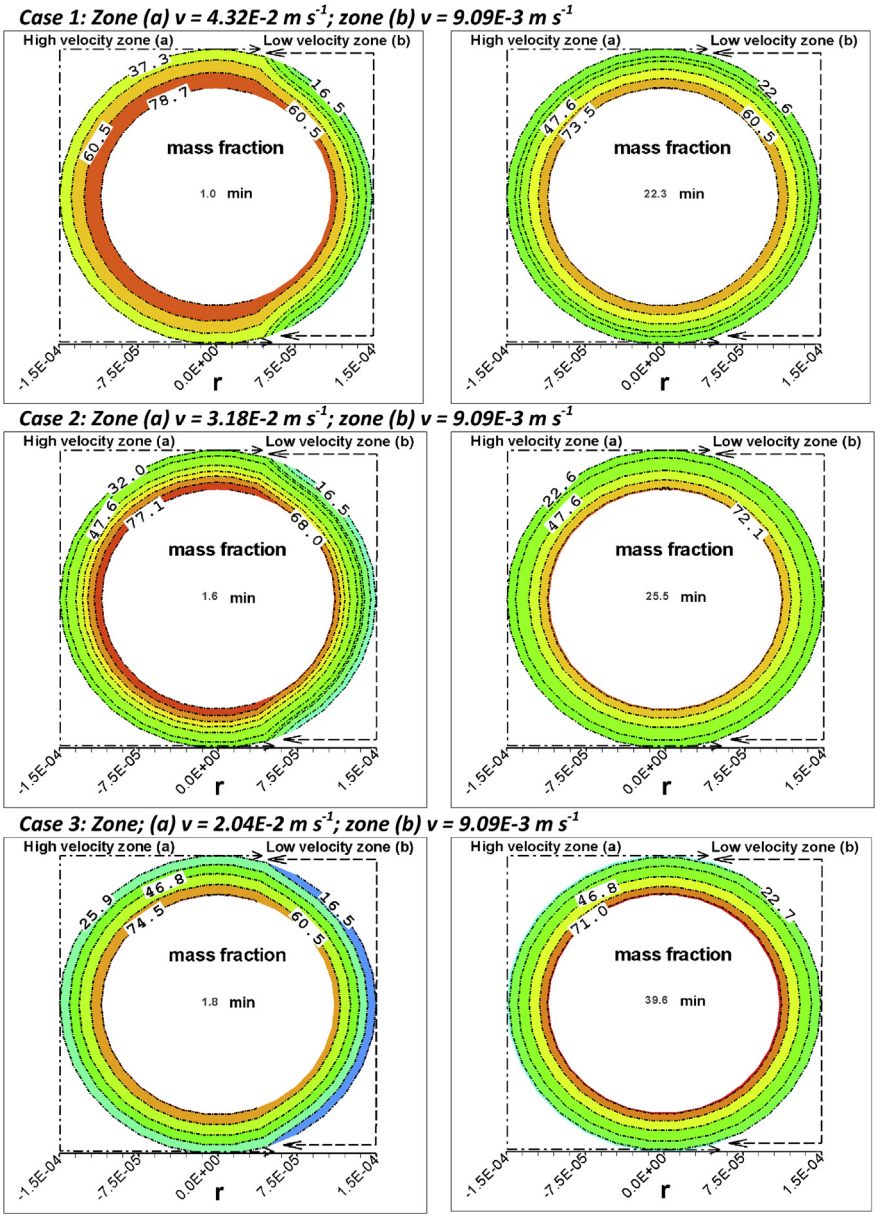

Fig. 6. Distribution of the mass fraction of gas (%w/w) inside a membrane used for osmotic distillation with higher external surface velocities in zone (a) and lower velocities in zone (b). The volumetric flux, the brine concentration and the temperature are 0.5 l/min, 33.13% w/w y 40 °C, respectively.

on its surface can be improved and thus enhance mass transfer and efficiency of the modules.

In future research, the mathematical model and the computational simulation can be extended to consider the momentum equations inside the membrane module. An algorithm that enables the coupling of momentum, energy and mass equations would allow to describe the velocity fields in the outside of the fibers with higher accuracy. Such a development, combined with the results presented

https://doi.org/10.1016/j.heliyon.2019.e01458

in this study, would allow for a more accurate calculation of mass transfer in OD processes.

7. Conclusions

A bi-dimensional mathematical model that includes UNIFAC and ASOG methods to obtain water activity at the interphases juice-membrane and membrane-brine was solved with the Finite Volume Method (FVM) to calculate the concentration of gas inside of a hydrophobic hollow fiber membrane used for OD of juices.

Simulations were carried out in two dimensions to include the effect of a non-uniform velocity field at the external surface of a hollow fiber of cylindrical shape. The velocity field has a direct effect on the mass advection coefficients that influence the mass transfer inside the membrane. The performed numerical simulation showed that it is possible to obtain higher or lower transmembrane fluxes depending on the velocity field that exists at the surface of the membrane. This velocity field can serve to improve the design of the cartridge that contains the hollow fibers and the shape of the fiber itself.

As noted in this article, the manufacturing of higher efficiency membrane modules is a continuous challenge. From this study, it can be concluded that to improve the description of the OD process, it is necessary to obtain the effective diffusion coefficient within the membrane, and to consider both the geometry of the hollow fibers and the effect on the velocities field over its surface.

Declarations

Author contribution statement

Carlos Zambra: Conceived and designed the experiments; Performed the experiments; Analyzed and interpreted the data; Contributed reagents, materials, analysis tools or data; Wrote the paper.

Funding statement

This work was supported by the Chilean National Commission for Scientific & Technological Research through the Project FONDECYT 1161093.

Competing interest statement

The authors declare no conflict of interest.

https://doi.org/10.1016/j.heliyon.2019.e01458

Additional information

No additional information is available for this paper.

References

Bergman, T.L., Lavine, A.S., Incropera, F.P., Dewitt, D.P., 2011. Fundamentals of Heat and Mass Transfer, seventh ed. Jhon Wiley & Sons.

Cassano, A., Drioli, E., 2007. Concentration of clarified kiwifruit juice by osmotic distillation. J. Food Eng. 79, 1397−1404.

Celere, M., Gostoli, C., 2005. Heat and mass transfer in osmotic distillation with brines, glycerol and glycerol-salt mixtures. J. Membr. Sci. 257, 99−110.

Cisse, M., Vaillant, F., Perez, A., Dornier, M., Reynes, M., 2005. Original Article the Quality of orange Juice Processed by Coupling Crossflow Microfiltration and Osmotic Evaporation, pp. 105−116.

Correa, A., Comesaña, J.F., Correa, J.M., Sereno, A.M., 1997. Measurement and prediction of water activity in electrolyte solutions by a modified ASOG group contribution method. Fluid Phase Equilib. 129, 267−283.

Dincer, C., Tontul, I., Topuz, A., 2016. A comparative study of black mulberry juice concentrates by thermal evaporation and osmotic distillation as influenced by storage. Innov. Food Sci. Emerg. Technol. 38, 57−64.

Gabelman, A., Hwang, S.T., 1999. Hollow fiber membrane contactors. J. Membr. Sci. 159, 61−106.

Hasanoğlu, A., Rebolledo, F., Plaza, A., Torres, A., Romero, J., 2012. Effect of the operating variables on the extraction and recovery of aroma compounds in an osmotic distillation process coupled to a vacuum membrane distillation system. J. Food Eng. 111, 632−641.

Kaya, R., Deveci, G., Turken, T., Sengur, R., Guclu, S., Koseoglu-Imer, D.Y., Koyuncu, I., 2014. Analysis of wall shear stress on the outside-in type hollow fiber membrane modules by CFD simulation. Desalination 351, 109−119.

Liguori, L., Russo, P., Albanese, D., Di Matteo, M., 2013. Evolution of quality parameters during red wine dealcoholization by osmotic distillation. Food Chem. 140, 68−75.

Luelf, T., Tepper, M., Breisig, H., Wessling, M., 2017. Sinusoidal shaped hollow fibers for enhanced mass transfer. J. Membr. Sci. 533, 302−308.

Motevalian, S.P., Borhan, A., Zhou, H., Zydney, A., 2016. Twisted hollow fiber membranes for enhanced mass transfer. J. Membr. Sci. 514, 586−594.

https://doi.org/10.1016/j.heliyon.2019.e01458

Patankar, S.V., 1991. Computational of Conduction and Duct Flow Heat Transfer. CRC Taylor & Francis Group.

Peres, M., Macedo, A., 1999. Prediction of thermodynamic properties using a modified UNIFAC model : application to sugar industrial systems. Fluid Phase Equilib. 158−160, 391−399.

Rana, D., Matsuura, T., 2010. Membrane transport models. In: Heldman, D.R., Moraru, C.I. (Eds.), Encyclopedia of Agriculture, Food and Biological Engineering, second ed. Taylor & Francis, New York, pp. 1041−1047.

Rana, D., Matsuura, T., Kassim, M.A., Ismail, A.F., 2015. Reverse osmosis membrane. In: Pabby, A.K., Rizvi, S.S.H., Sastre, A.M. (Eds.), Handbook of Membrane Separations: Chemical, Pharmaceutical, Food, and Biotechnological Applications, second ed. Taylor & Francis, Press, Boca Raton, FL, pp. 35−52.

Rana, D., Matsuura, T., Sourirajan, S., 2014. Physicochemical and engineering properties of food in membrane separation processes. In: Rao, M.A., Rizvi, S.S.H., Datta, A.K., Ahmed, J. (Eds.), Engineering Properties of Foods. Taylor & Francis, Boca Raton, Fl, pp. 1041−1047.

Ruiz Salmón, I., Janssens, R., Luis, P., 2017. Mass and heat transfer study in osmotic membrane distillation-crystallization for CO2valorization as sodium carbonate. Separ. Purif. Technol. 176, 173−183.

Savaş Bahçeci, K., Gül Akillioglu, H., Gökmen, V., 2015. Osmotic and membrane distillation for the concentration of tomato juice: effects on quality and safety characteristics. Innov. Food Sci. Emerg. Technol. 31, 131−138.

Serrano, S.E., 2004. Modeling infiltration with approximate solutions to Richard's equation. J. Hydrol. Eng. - ASCE 9, 421−432.

Vaillant, F., Jeanton, E., Dornier, M., Brien, G.M.O.Õ., Reynes, M., Decloux, M., 2001. Concentration of passion fruit juice on an industrial pilot scale using osmotic evaporation. J. Food Eng. 47, 195−202.

Valdés, H., Romero, J., Saavedra, A., Plaza, A., Bubnovich, V., 2009. Concentration of noni juice by means of osmotic distillation. J. Membr. Sci. 330, 205−213.

Woods, J., Pellegrino, J., 2013. Heat and mass transfer in liquid-to-liquid membrane contactors: design approach and model applicability. Int. J. Heat Mass Transf. 59, 46−57.

Zambra, C.E., Moraga, N.O., 2013. Heat and mass transfer in landfills: simulation of the pile self-heating and of the soil contamination. Int. J. Heat Mass Transf. 66, 324−333.

 https://doi.org/10.1016/j.heliyon.2019.e01458

Zambra, C.E., Muñoz, J.F., Moraga, N.O., 2015. A 3D coupled model of turbulent forced convection and diffusion for heat and mass transfer in a bioleaching process. Int. J. Heat Mass Transf. 85, 390−400.

Zambra, C.E., Romero, J., Pino, L., Saavedra, A., Sanchez, J., 2014. Concentration of cranberry juice by osmotic distillation process. J. Food Eng. 144, 58−65.

https://doi.org/10.1016/j.heliyon.2019.e01458